

Threshold of motion and orientation of bivalve shells under current flow

Felipe Rafael Secco da Silva^{1*} , Ana Luiza de Oliveira Borges¹ , Elírio Ernestino Toldo Jr.² , Cristiano Fick¹ , Eduardo Puhl¹ , Vinícius Carbone Bernades Oliveira³ , Francisco Eduardo Gomes da Cruz⁴ 

Abstract

Disarticulated shells of three bivalve mollusk species (*Anomalocardia brasiliiana*, *Codakia orbicularis*, and *Divaricella quadrisulcata*) were experimentally tested in laboratory flumes to determine the threshold of motion and final orientation of the valves. A total of 150 current flow experiments were conducted on single shells resting on a fixed sand bed. This study demonstrated that shells in the convex-up position are more resistant to flow when the umbo is pointing downstream rather than upstream. Moreover, species with higher frontal areas were more likely to be entrained at lower flow velocities. Results of dimensionless shear stress exhibited values far below the threshold of grains movement for beds of uniform roughness (Shields curve). It was observed that circular shells in convex-up positions were mostly orientated with the umbo pointing downstream. Conversely, elliptical shells in convex-up position tended to align their longer axis parallel to the flow with the posterior side of the valve pointing downstream. These results are not only directly applicable in interpretations of incipient shell motions and in paleocurrent analyses from field and sample data, but also support construction of accurate geological models.

KEYWORDS: bivalve shells; shell orientation; threshold of motion; flume experiments; unidirectional flow.

INTRODUCTION

Dense shell accumulations (i.e., coquinas, shell pavements, or shell beds) have been studied in recent decades by many researchers because of their importance as petroleum reservoirs and recurrent occurrence in both ancient deposits (Carvalho *et al.* 2000, Tavares *et al.* 2015, Muniz and Bosence 2018, Oliveira *et al.* 2019, Rodrigues *et al.* 2022) and modern coastal settings (Calliari and Klein 1993, Jahnert *et al.* 2012, Weill *et al.* 2013, Charó *et al.* 2014). The genesis of mollusk-dominated, shell-rich deposits is frequently associated with coastal and shallow water sedimentary environments in both marine and lacustrine settings, where waves and currents are the main processes responsible for sediment reworking and

transport (Fick *et al.* 2020). The threshold of motion and shell orientation provide important information about how these skeletal grains are transported and sorted by flow. In paleoenvironmental analysis, the shell position and its degree of fragmentation have been used to infer the direction (Nagle 1967, Wendt 1995, Radley 2011) and energy (Trewin and Welsh 1972, Schwartz and Graham 2015) of the paleoflow.

The physical parameters of the shells, such as mass, shape, size, and surface roughness, control their movement behavior (Vogel 1994). Chattopadhyay *et al.* (2013) revealed that fresh shells with rough surfaces are more easily transported than older reworked shells. The asymmetry of the shells is another distinguishable property. Shape asymmetries contribute to ease of transport because they generate unstable pressure fields around the shell (Olivera and Wood 1997). The orientation of the shell convexity in a flow dictates its stability; the convex-up posture is more stable than the convex-down one (Nagle 1967, Brenchley and Newal 1970, Allen 1984, Dey 2003, Diedericks *et al.* 2018, Fick *et al.* 2020). The initial umbo position also affects the entrainment of the shells (Dey 2003, Chattopadhyay *et al.* 2013, Diedericks *et al.* 2018). Futterer (1982) reported that circular-shaped shells transported in a convex-up position by currents require a greater range of transport velocities when the umbo faces downstream than when it points upstream.

To better understand the hydrodynamic behavior of shells, this study aimed to investigate the incipient motion conditions and orientation patterns of bivalve shells under currents through physical modeling experiments. Based on the results, insights

¹Universidade Federal do Rio Grande do Sul, Instituto de Pesquisas Hidráulicas, Núcleo de Estudos de Correntes de Densidade – Porto Alegre (RS), Brazil. E-mails: felipersecco@hotmail.com, alborges@iph.ufrgs.br, cristiano.fick@ufrgs.br, eduardo.puhl@ufrgs.br

²Universidade Federal do Rio Grande do Sul, Instituto de Geociências, Centro Estudos de Geologia Costeira e Oceânica – Porto Alegre (RS), Brazil. E-mail: toldo@ufrgs.br

³Centro de Pesquisas Leopoldo Américo Miguez de Mello, Petróleo Brasileiro S.A. – Rio de Janeiro (RJ), Brazil. E-mail: viniciuscarbone@petrobras.com.br

⁴Petróleo Brasileiro S.A. – Rio de Janeiro (RJ), Brazil. E-mail: fcruz@petrobras.com.br

*Corresponding author.



on taphonomic signatures (shell orientation, *sensu* Kidwell *et al.* 1986), bioclastic sediment sorting, and paleocurrent behavior are proposed and discussed in a geological context.

Threshold of motion

The study of the threshold of motion is associated with the critical condition under which a grain is likely to begin moving. This condition is reached when the sum of the flow drag (F_D) and lift (F_L) forces are equal (or on the threshold) to the particle's submerged weight (W). In addition, the bed slope angle (ψ) and the repose angle (ψ_r) of the bed particles must be considered. The shear stress near the bed (τ_b) can be related to F_D through the Eq. 1:

$$F_D = C_1 \tau_b D^2 \quad (1)$$

Where:

- C_1 = a coefficient that considers the drag and lift effects;
- τ_b = the shear stress near the bed (Pa);
- D = the particle diameter (m).

The submerged weight (W) is given by the Eq. 2:

$$W = C_2 (\gamma_s - \gamma) D^3 \quad (2)$$

Where:

- C_2 = a geometric coefficient;
- γ_s = the specific weight of the grain ($N\ m^{-3}$);
- γ = the specific weight of the water ($N\ m^{-3}$).

Substituting W and F_D for their respective expressions, the balance of these forces for the threshold of motion condition is given by the Eq. 3:

$$C_2 (\gamma_s - \gamma) D^3 \cos \psi \operatorname{tg} \psi_r = C_1 \tau_b D^2 + C_2 (\gamma_s - \gamma) D^3 \operatorname{sen} \psi \quad (3)$$

For a horizontal bed, the above equation can be rewritten as follows (Eq. 4):

$$\frac{\tau_{b,cr}}{(\gamma_s - \gamma) D} = \frac{C_2}{C_1} \operatorname{tg} \psi_r \quad (4)$$

The left term of the expression in the above equation is the nondimensional Shields parameter (θ_{cr}), which expresses the ratio between the hydrodynamic forces and the submerged weight.

Shields (1936), based on unidirectional flow experiments with spherical inorganic (barite and granite sand) and organic (amber and coal fragments) grains, defined an experimental curve of the θ_{cr} parameter versus the grain Reynolds number (Re^*). Re^* is a dimensionless parameter that expresses the effects of particles on the flow boundary layer, given by the Eq. 5:

$$Re^* = \frac{u_* D}{\nu} \quad (5)$$

Where:

- u_* = the shear velocity ($= \sqrt{\frac{\tau_b}{\rho}}$);
- ν = the kinematic viscosity ($m^2\ s^{-1}$).

Ever since it was developed, the Shields (1936) curve has been used for siliciclastic grains (Miller *et al.* 1977, Buffington and Montgomery 1997), calcareous fragments (Paphitis *et al.* 2002, Smith and Cheung 2004), and nonfragmented shells (Diedericks *et al.* 2018, Fick *et al.* 2020) in initiation of movement studies.

MATERIALS AND METHODS

The flume experiments performed in this work were carried out under two different scenarios: single-shell and shell-bed experiments. A summary of the methodology is provided in Table 1.

Single-shell experiments

Disarticulated and nonfragmented valves of three bivalve shell species were used in the single-shell experiments. The shell species were *Anomalocardia brasiliana*, *Codakia orbicularis*, and *Divaricella quadrisulcata*. These species are frequently found along the southeastern Brazilian coast. All specimens were obtained from Holocene back-barrier deposits (Fornari 2010) on the Jaguaruna coastal plain, Santa Catarina, Brazil.

A group of valves of different sizes was selected for each species (Fig. 1). Moreover, *Anomalocardia brasiliana* (elliptical

Table 1. Methodology summary for the single-shell and shell-bed experiments.

	Single-shell experiments	Shell-bed experiments
Goals	<ul style="list-style-type: none"> • Shell final orientation • Threshold of motion condition 	<ul style="list-style-type: none"> • Shell final orientation
Valves initial position	<ul style="list-style-type: none"> • Convex-up: umbo downstream • Convex-up: umbo upstream 	<ul style="list-style-type: none"> • Concave-up: umbo randomly oriented
Species	<ul style="list-style-type: none"> • <i>Anomalocardia brasiliana</i> • <i>Codakia orbicularis</i> • <i>Divaricella quadrisulcata</i> 	<ul style="list-style-type: none"> • <i>Anomalocardia brasiliana</i>

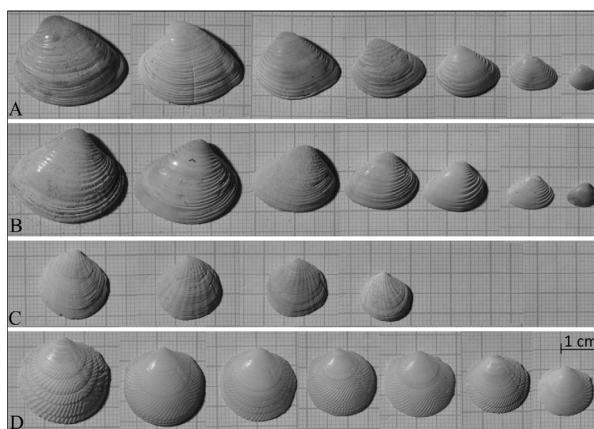


Figure 1. Shells used in single shell experiments. (A) *Anomalocardia brasiliana*, left valves; (B) *Anomalocardia brasiliana*, right valves; (C) *Codakia orbicularis*; (D) *Divaricella quadrisulcata*.

asymmetric shape) shells were identified as left and right valves (Fig. 2). For *Codakia orbicularis* and *Divaricella quadrisulcata*, this discrimination was not needed because they are circular shells with both valves bilaterally symmetrical.

Some physical shell properties were accurately determined and are presented in Table 2. Shell mass (m), volume

(V), and density (ρ) were measured with a scale (0.01 g precision) and a pycnometer (Hubbard-type, 25 ml). The shells' longest, intermediate, and minor axes (a, b, and c, respectively) were measured with a caliper (0.02 mm precision). The sieve diameter (D_{sv}) was calculated using the Church *et al.*'s (1987) formula (Eq. 6):

$$\frac{D_{sv}}{b} = \frac{1}{\sqrt{2}} \left[1 + \left(\frac{c}{b} \right)^2 \right]^{0.5} \tag{6}$$

The nominal diameter (D_n), which is the diameter of a sphere with the same volume as the shell, was calculated using the Eq. 7:

$$D_n = \left(\frac{6V}{\pi} \right)^{\frac{1}{3}} \tag{7}$$

The projected area of the shell (S_{ac}) on the plane formed by axes (a) and (c) was measured by a photograph analysis using AUTOCAD® software.

To illustrate the convexity and thickness distribution through the shell, one valve of each species was cut into five sections (Fig. 2C). A valve from *Anomalocardia brasiliiana* ($D_{sv} = 17.31$ mm) had an average thickness of 1.8 mm, and the anterior side of the shell was 2.4 mm thick on average.

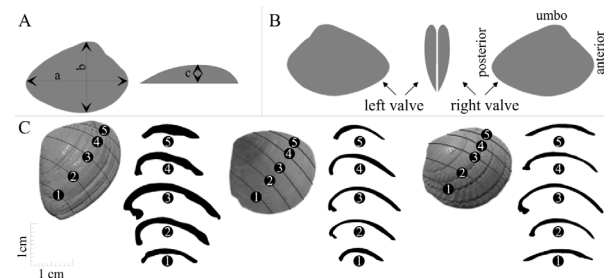


Figure 2. Shape of bivalve shells. (A) Scheme of shell axis orientation. (a) and (b) are the base axes, (c) is the shell height. (B) Scheme of the adopted convention for asymmetrical valve sides. (C) Cross sections on the plane formed by the axes (b) and (c). From left to right: *Anomalocardia brasiliiana* specimen ($D_{sv} = 17.31$ mm), *Codakia orbicularis* specimen ($D_{sv} = 12.75$ mm), *Divaricella quadrisulcata* specimen ($D_{sv} = 15.99$ mm). The scale in the lower left corner only applies for the cross sections.

Table 2. Mass, density, shell's axes sizes, sieve (D_{sv}) and nominal (D_n) diameters, and projected area (S_{ac}) on a plane composed by the axes (a) and (c).

Species	Sample number	Valve side	Mass ($\text{kg} \times 10^{-3}$)	Density ($\text{kg m}^{-3} \times 10^3$)	Axis (mm)			D_{sv} (mm)	D_n (mm)	S_{ac} (mm^2)
					a	b	c			
<i>Anomalocardia brasiliiana</i>	1		3.06	2.62	28.5	23.2	9.0	18.9	13.2	166.2
	2		2.08		26.1	21.1	8.0	17.1	11.5	130.5
	3		1.20		21.5	17.2	6.7	14.0	9.6	98.4
	4	Left	0.66		18.3	15.0	5.3	11.9	7.8	62.1
	5		0.53		16.0	13.0	4.8	10.4	7.3	50.6
	6		0.16		12.2	8.9	3.2	7.1	4.9	27.6
	7		0.01		7.7	6.0	2.5	5.0	1.8	4.4
	8		3.15		29.0	24.0	9.0	19.4	13.3	186.7
	9		1.67		26.4	21.8	7.8	17.4	10.7	132.4
	10		1.13		21.5	17.2	6.8	14.1	9.4	100.1
	11	Right	0.72		18.7	14.5	5.5	11.7	8.0	73.6
	12		0.56		15.8	12.7	5.0	10.4	7.4	56.6
	13		0.13		12.0	8.7	3.0	6.9	4.6	24.8
	14		0.01		7.8	6.3	2.5	5.2	2.0	6.6
<i>Codakia orbicularis</i>	15		0.64	2.66	17.2	17.3	5.5	13.5	7.7	61.8
	16		0.60		16.3	16.0	5.1	12.5	7.6	59.0
	17		0.46		15.3	14.7	4.5	11.4	6.9	53.0
	18		0.36		12.8	12.3	4.1	9.7	6.3	43.0
<i>Divaricella quadrisulcata</i>	19		1.05	2.61	22.3	21.5	7.1	16.9	9.0	110.8
	20		0.79		20.0	19.7	6.1	15.3	8.2	89.1
	21		0.60		19.1	18.5	5.7	14.3	7.5	72.7
	22		0.48		17.2	16.5	4.6	12.6	6.9	53.3
	23		0.41		17.7	16.6	4.9	12.8	6.6	57.8
	24		0.28		15.8	14.9	4.3	11.4	5.8	46.4
	25		0.16		14.6	12.5	3.7	9.6	4.9	29.5

The *Codakia orbicularis* ($D_{sv} = 12.75$ mm) and *Divaricella quadrisulcata* ($D_{sv} = 15.99$ mm) specimens had average thicknesses of 1.06 and 0.94 mm, respectively; both species had slight thickness variations between the posterior and anterior sides (less than 0.3 mm).

Experiments were conducted on a masonry flume (Fig. 3) measuring 11 m long, 0.4 m wide, and 0.5 m in height. The flume bed had a gentle slope (4/1,000), and its surface was a compound of well-sorted fixed sand (mean $D_{sv} = 0.8$ mm). At the upstream end, the flume was equipped with a rectangular weir (Fig. 3B) to determine the discharge (Q). A depth gauge (0.0001 m precision) was coupled to the weir to determine the height of water (wh) flowing over it. The discharge (Q) value is given by the Eq. 8:

$$Q = \frac{[0.8919 + 0.137752 \left(\frac{wh}{100} \right) + 0.011]}{(wh + 0.01)^{-1.5}} \quad (8)$$

Four depth gauges (0.001 m precision) were fixed at 1.5, 4, 4.8, and 6 m (black arrows in Fig. 3) from the beginning of the bed to measure the flow depth (h).

The shell's incipient motion condition was tested in two initial positions: convex-up with the umbo facing upstream and convex-up with the umbo pointing downstream. For each experiment, the flume was filled with water at a low current velocity, and a single shell was positioned at a specific point (Fig. 3C). By opening an upstream valve (Fig. 3A), the flow was increased until the shell started its movement. Subsequently, the flow depth and discharge were measured. This procedure was repeated three times for each shell at both the initial positions. The adopted criterion for incipient motion was considered to have been reached when the shell moved at least 0.1 m.

In preliminary experiments, shells, when entrained with the umbo initially facing upstream, turned on their horizontal plane to reach a more stable position and then stopped moving. In these cases, the final orientation of the valves was determined using a protractor. These measurements were taken along the shell's intermediate axis, and the recorded data showed the direction of the umbo. In experiments where the umbo was facing downstream, it was not possible to measure the shell's final orientation because the shells did not stop their movement until reaching the downstream end of the flume.

All experiments were conducted in a uniformly stable flow regime. The mean flow velocity (U) for the threshold of motion conditions was calculated using continuity (Eq. 9):

$$U = QA^{-1} \quad (9)$$

Where:

A = the wet area (m^2);

Q = the discharge ($m^3 s^{-1}$).

In addition, the mean bed shear stress for the incipient motion condition ($\tau_{b,cr}$) was determined using the Eq. 10:

$$\tau_{b,cr} = \gamma \frac{A}{P} S \quad (10)$$

Where:

γ = the specific weight of water (Nm^{-3});

P = the wet perimeter (m);

S = the flume slope.

Shell-bed experiments

In the shell-bed experiments, an amount of 1 kg sample of nonfragmented valves from the *Anomalocardia brasiliiana* species was used. The sample D_{sv} value ranged from 3.8 to 22.25 mm (Fig. 4).

Experiments were conducted in a 4 m long, 0.12 m wide, and 0.5 m tall recirculating glass flume (Fig. 5). The recirculating system connected the pump to a lower reservoir. In addition, the flume had a trough in its center (0.02 m deep and 0.6 m long). The unconsolidated material did not return to the pipe owing to the presence of a net in the downstream box. A calibrated valve and two staff gauges (0.001 m precision) measured the discharge (Q) and flow depth (h), respectively.

Before each experiment, the flume was completely filled with water, and then the entire 1 kg *Anomalocardia brasiliiana* valve sample was lowered into the trough area, filling all available space. Because of this procedure, the valves lay on the bed in a concave-up position (Middleton 1967, Allen 1984, Li *et al.* 2020). Subsequently, the water level was slowly dropped to the predetermined flow height. The experiment started when the upstream valve (Fig. 5D) was opened with the calibrated valve (Fig. 5C) already adjusted. The experiment lasted for 20 min. This time was established in preliminary

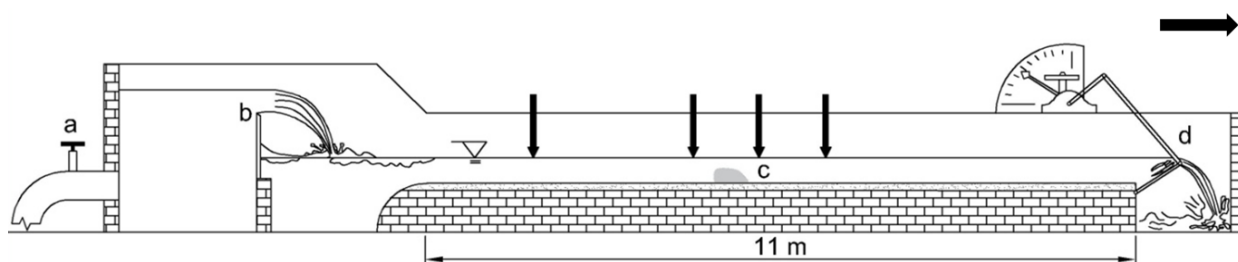


Figure 3. Cross section of the flume used on single shell experiments (not to scale): (a) water feeding valve, (b) rectangular weir, (c) initial shell position, (d) downstream floodgate. Vertical black arrows show the position of depth gauges. Horizontal black arrow points in the flow direction.

tests, in which it was verified that there was no significant transport after this period.

After each run, a top-shell-bed photograph was taken. These photographs were obtained using a digital camera equipped with a CARL ZEISS T*1.4/85 mm planar lens. Subsequently, all shells were collected for use in the next experiment.

To investigate the orientation pattern of the right and left *Anomalocardia brasiliiana* valves, eight experiments were conducted. The mean flow velocities used were 0.48, 0.52, 0.54, and 0.57 ms⁻¹ with each velocity having one repetition.

The shell-bed photographs taken after the experiments were analyzed to measure the shell orientation. In this analysis, the edges 0.1 m from both ends were discarded due to the transition between fixed and mobile beds. The bed area was split into two in a checkered pattern (Fig. 6). The measurements were computed for all shells in a convex-up position that were partially or fully inside the brown squares. The orientation data were taken along the shell's

intermediate axis with the recorded data exhibiting the direction of the umbo.

RESULTS

Threshold of motion

The critical bed shear stresses for the single-shell experiments were calculated using Eq. 3. The relationship between the particle size (D_n and D_{sv}) and this parameter is shown in Fig. 7. The mean flow depth and velocity values are presented in Table 3. There were significant disparities in the critical shear stress values for the experiments, in which shells with the umbo facing upstream had lower values than those facing downstream, demonstrating that shells in the second situation exhibited major resistance to transportation.

The regressions showed similar trends for both characteristic diameters, as shown in the graphs. A positive correlation existed between the size and critical shear stress ($\tau_{b,cr}$) when the umbo was facing downstream. Under these conditions, *Anomalocardia brasiliiana* and *Divaricella quadrisulcata* showed strong correlations, with the regression analyses ($\tau_{b,cr}$ versus D_n) having coefficients of determination (R^2) of 0.91 and 0.87, respectively. With a Pearson coefficient of 0.88 ($R^2 = 0.77$), the species *Codakia orbicularis* had a lower correlation with the critical shear stress than did the other two species, yet the (R^2) value is still reasonable.

For the situation in which the umbo faces upstream, the graphs (Fig. 7) from *Anomalocardia brasiliiana* and *Divaricella*

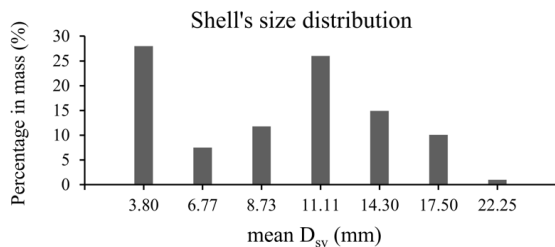


Figure 4. Sieve grain size distribution of a sample of *Anomalocardia brasiliiana* valves.

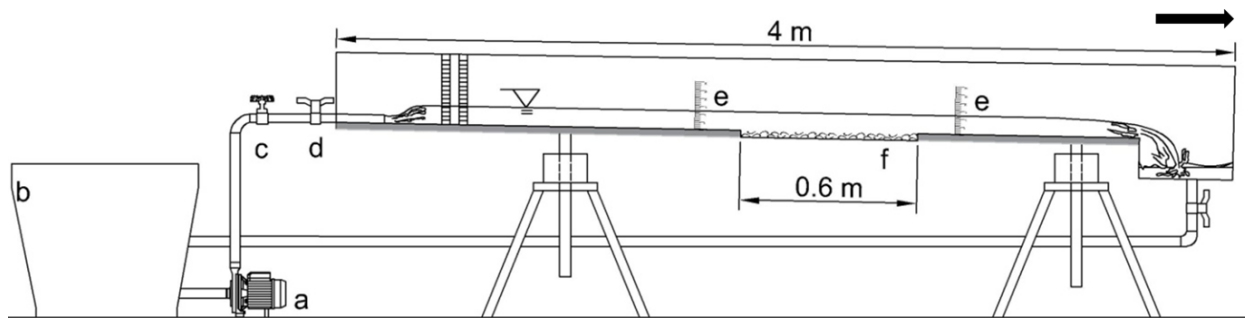


Figure 5. Cross section of the shell bed experiments flume (not to scale): (a) pump, (b) lower reservoir, (c) calibrated valve, (d) upstream valve, (e) staff gauges, (f) trough. Black arrow indicates the flow direction.

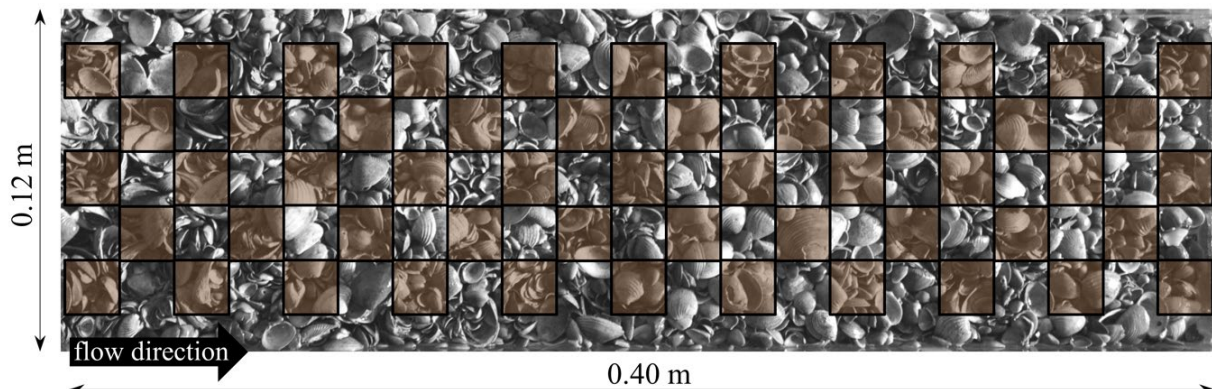


Figure 6. Shell bed photograph of the central trough area. The brown squares represent the analysis area.

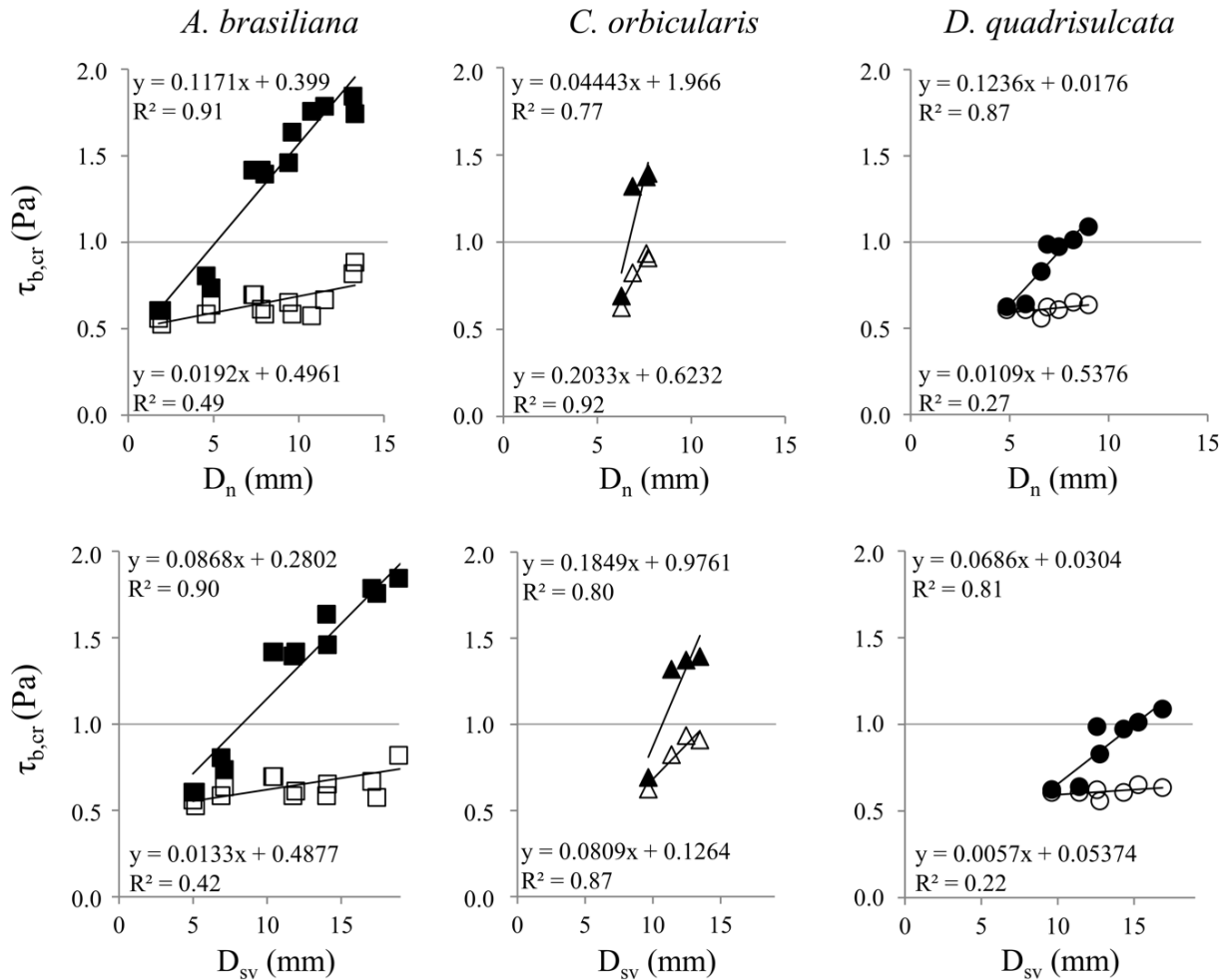


Figure 7. Critical shear stress as a function of the shell’s diameter. From left to right the graphs are for the species *Anomalocardia brasiliana*, *Codakia orbicularis*, and *Divaricella quadrisulcata*, respectively. Upper panel: shells size represented by the nominal diameter (D_n). Lower panel: shells size represented by the sieve diameter (D_{sv}). Solid symbols represent the umbo initially pointing downstream and open symbols for the umbo pointing upstream.

quadrisulcata show that the thresholds of motion were not a function of the shell size. Although the correlation was still positive, small and large shells had similar $\tau_{b,cr}$ values.

For small shells (D_{sv} from 4 to 8 mm), the $\tau_{b,cr}$ values were very similar for both the initial umbo orientations tested in this work. However, in the case of larger shell sizes, the $\tau_{b,cr}$ ratios between the umbo pointing downstream and pointing upstream varied considerably among the different species: 2.67 for *Anomalocardia brasiliana* (D_n = 11.5 mm/D_{sv} = 17.06 mm); 1.53 for *Codakia orbicularis* (D_n = 7.7 mm/D_{sv} = 13.47 mm); and 1.71 for *Divaricella quadrisulcata* (D_n = 9 mm/D_{sv} = 16.86 mm).

The size range that includes all these species (D_{sv} from 9.5 to 14 mm) allows comparisons between individual species with respect to their thresholds of motion. In this range, the average $\tau_{b,cr}$ values acquired with the umbo facing upstream show no important differences between species: 0.63 Pa for *Anomalocardia brasiliana*, 0.82 Pa for *Codakia orbicularis*, and 0.60 Pa for *Divaricella quadrisulcata*. However, when the umbo was facing downstream for the *Divaricella quadrisulcata* species, the average $\tau_{b,cr}$ value (0.77 Pa) was significantly lower than that of the other species. *Anomalocardia brasiliana*

and *Codakia orbicularis* had average $\tau_{b,cr}$ values of 1.49 and 1.19 Pa, respectively.

Shields parameter

The critical Shields parameter for the incipient motion condition (θ_{cr}) was calculated from the left term of Eq. 4 using the shell D_{sv} as the characteristic dimension of the shell, which was then plotted (Fig. 8) as a function of the grain Reynolds number (Re*). Considering that Re* is related to the viscous effects of the flow developed on a bed of uniform roughness, Wiberg and Smith (1987) and Ramsdell and Miedema (2010) recommended that the mean diameter of the bed be used to calculate the grain Reynolds number in Eq. 5. For all experiments performed in this work, the mean sieve diameter (D_{sv} = 0.8 mm) of the glued sand bed was used in the Re* evaluation, as previously described by Diedericks *et al.* (2018).

As observed in the critical shear stress results, the θ_{cr} values were also larger for the case when the umbo faced downstream, ranging from 3.37×10^{-3} to 8.19×10^{-3} , whereas in the upstream case, the values varied from 1.98×10^{-3} to 6.73×10^{-3} . Notably, all data points plotted well below the Shields (1936) curve and Fick *et al.* (2020) envelope.

Table 3. Mean values of velocity (U), flow depth (h), and critical shear stress ($\tau_{b,cr}$).

Sample number	Umbo upstream			Umbo downstream		
	h (m)	U (ms ⁻¹)	$\tau_{b,cr}$ (Pa)	h (m)	U (ms ⁻¹)	$\tau_{b,cr}$ (Pa)
Anomalocardia brasiliiana						
1	0.024	0.43	0.82	0.064	0.71	1.84
2	0.019	0.35	0.67	0.061	0.70	1.79
3	0.017	0.29	0.59	0.055	0.66	1.64
4	0.017	0.31	0.61	0.046	0.61	1.42
5	0.020	0.36	0.70	0.046	0.61	1.42
6	0.018	0.34	0.64	0.021	0.37	0.74
7	0.016	0.28	0.56	0.017	0.27	0.61
8	0.026	0.45	0.88	0.059	0.69	1.74
9	0.016	0.29	0.58	0.060	0.70	1.76
10	0.019	0.34	0.65	0.047	0.62	1.46
11	0.017	0.29	0.59	0.045	0.60	1.39
12	0.020	0.36	0.70	0.046	0.61	1.42
13	0.017	0.29	0.59	0.024	0.40	0.81
14	0.015	0.25	0.53	0.017	0.27	0.61
Codakia orbicularis						
15	0.027	0.44	0.91	0.045	0.60	1.39
16	0.028	0.44	0.94	0.044	0.60	1.37
17	0.024	0.40	0.82	0.044	0.58	1.32
18	0.018	0.34	0.62	0.020	0.35	0.69
Divaricella quadrisulcata						
19	0.018	0.34	0.64	0.033	0.52	1.09
20	0.019	0.34	0.65	0.031	0.48	1.01
21	0.017	0.33	0.61	0.029	0.46	0.97
22	0.018	0.34	0.62	0.030	0.48	0.99
23	0.016	0.28	0.56	0.024	0.42	0.83
24	0.017	0.33	0.61	0.018	0.34	0.64
25	0.017	0.33	0.61	0.018	0.33	0.62

Regarding the highest critical Shields parameter values for the different species, *Divaricella quadrisulcata* was less resistant to the flow action, registering a θ_{cr} value equal to 4.71×10^{-3} . *Anomalocardia brasiliiana* and *Codakia orbicularis*, by contrast, were hydrodynamically more stable, as expressed by correspondingly higher motion threshold values ($\theta_{cr} = 8.19 \times 10^{-3}$ and 6.96×10^{-3} , respectively).

The results of θ_{cr} were also compared with the Ramsdell and Miedema (2010) curves for the prediction of the incipient motion of nonuniform particles in a uniform sand bed with variable roughness. The curves indicate that the ratios between the nonuniform particle diameter (D) and average bed roughness (k_s) are equal to 6 and 20. Following Fisher *et al.* (1983) and Diedericks *et al.* (2018), D was chosen to be equal to some characteristic shell diameter (shell $D_{sv} = D$), and k_s is equal to the diameter of the sand bed particles (bed particles $k_s = 0.8$ mm). The D/k_s ratios between all shell sizes studied in this research and the fixed sand bed stayed between 6.23 and 24.20. Almost all

shell data points were above the lowest curve ($D/k_s = 20$) of Ramsdell and Miedema (2010), and only for *Divaricella quadrisulcata* did no θ_{cr} value lie above the upper curve ($D/k_s = 6$).

In addition, Fig. 8 presents the θ_{cr} values calculated from the critical shear stress reported by Dey (2003) and Diedericks *et al.* (2018) for the threshold of motion of single shells under currents on a fixed sand bed (convex-up position/umbo facing downstream). All data from these authors have D/k_s ratios higher than 15 and θ_{cr} values far below the Shields (1936) curve.

Orientation: single-shell experiments

The valve orientations in the single-shell experiments, in which the umbo was initially pointing upstream, were computed for all the investigated species. In these experiments, the umbo orientation was controlled by the flow and shell morphology because the sand bed roughness was insignificant when compared to the shell size.

The rose diagrams (Fig. 9) show the final umbo orientations for all the specimens. The circular-shaped shell species (*Codakia orbicularis* and *Divaricella quadrisulcata*) presented a random orientation pattern. In contrast, the asymmetrical elliptical species, *Anomalocardia brasiliiana*, exhibited a bimodal pattern when the orientation of the right valves was compared with that of the left valves.

Anomalocardia brasiliiana showed a trend in which the right valve rotated counterclockwise, with the umbo orientation tending to point toward the right margin of the flume (270°), whereas the left valve rotated in the opposite direction and pointed the umbo toward the left margin. As shown in Fig. 9, all observations fit this pattern. Although the rotation motion occurred chaotically for the circular shells, it can be seen that *Codakia orbicularis* was mostly located in the second and third quadrants (Fig. 9), indicating that the umbo tended to point in a downstream orientation. In contrast, *Divaricella quadrisulcata* remained in a position near the starting umbo orientation (0°), probably because the shells of this species stopped their motion before a larger rotation.

Orientation: shell-bed experiments

The final orientation of the *Anomalocardia brasiliiana* valves in the shell-bed experiments presented a more random picture compared to the single-shell experiments. This probably occurred because in this scenario, the hydrodynamically stable position of the shell was impaired by the neighboring shells that compounded the bed.

The rose diagrams (Fig. 10) show the umbo shell orientations that were in a convex-up position on the shell bed. Although these data have a large range of umbo directions, they agree with the tendency observed in the single-shell experiments. Thus, 62% of the umbo orientations (Table 4) on average point toward the right flume margin (third and fourth quadrants). This tendency was below 50% only in experiments 5 and 7. The largest number (77%) of right valves that followed this behavior was observed in experiment 2. In addition, as seen in the single-shell experiments, the results for the left valves show that, on average, 76% of the umbos pointed toward the left flume margin (first and second quadrants).

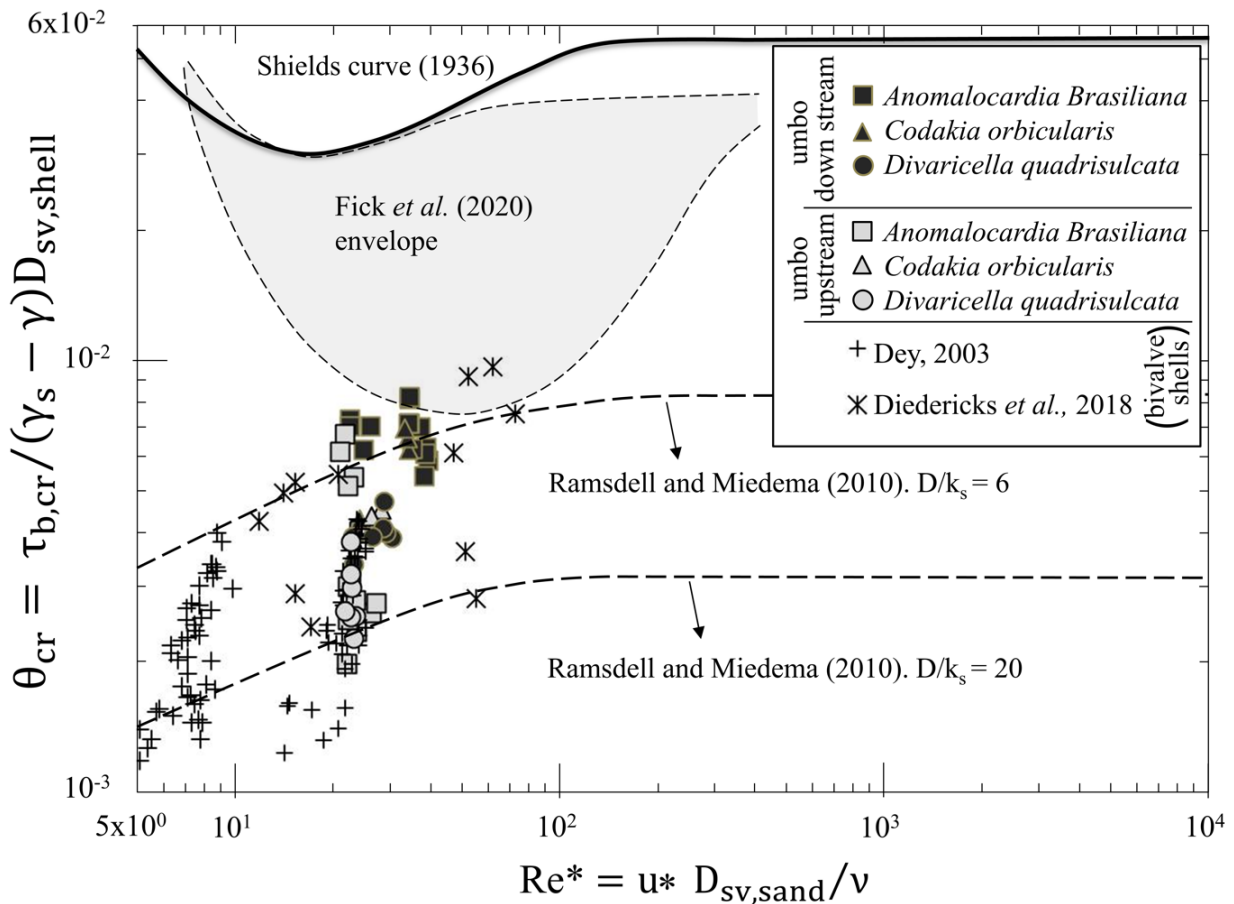


Figure 8. Shields diagram (θ_{cr} versus Re^*) of the threshold of motion datasets from the bivalve shells *Anomalocardia brasiliana*, *Codakia orbicularis*, and *Divaricella quadrisulcata*. The data points include the experimental results for nonfragmented bivalve shells under currents from Dey (2003) and Diedericks *et al.* (2018). The Ramsdell and Miedema (2010) and Fick *et al.* (2020) curves ($D/k_s = 6$ and 20) are plotted together with the Shields (1936) curve.

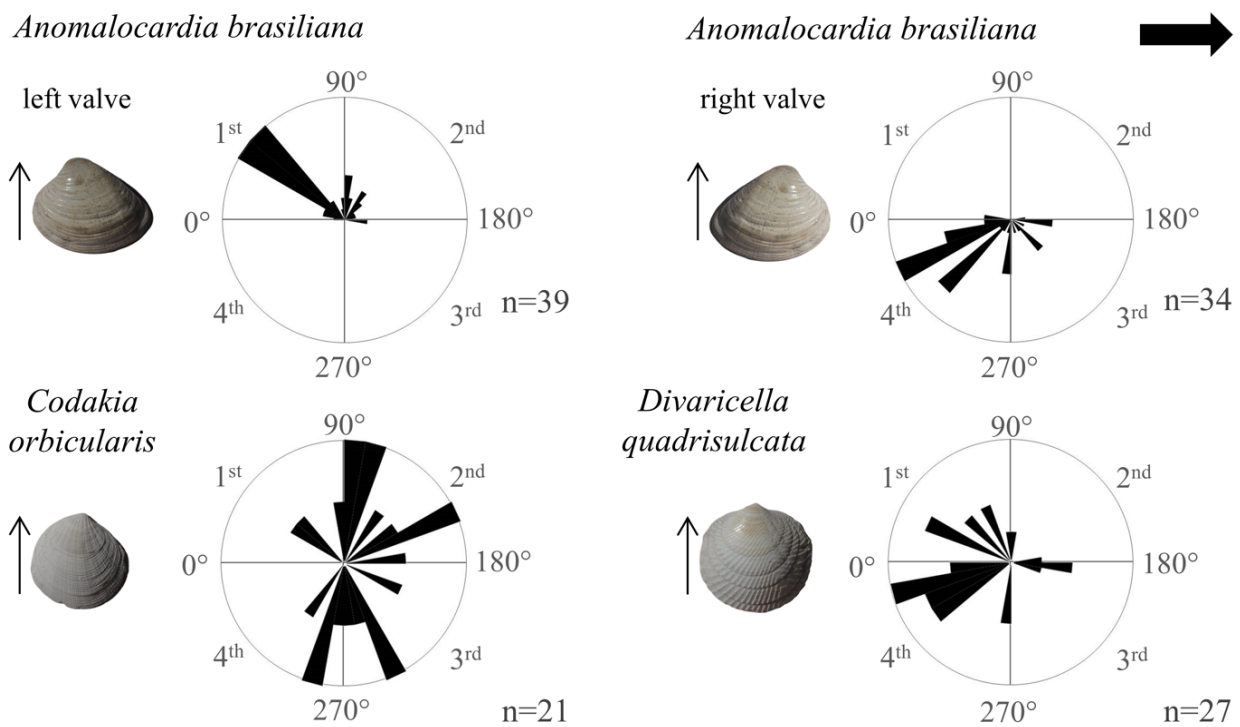


Figure 9. Umbo orientation of single shells resting in a fixed sand bed. Top, the elongate species *Anomalocardia brasiliana* discriminated between right and left valves. Below, the diagrams from the circular shells species: *Codakia orbicularis* and *Divaricella quadrisulcata*. n: number of measures; 0°: initial umbo position (upstream). The thin black arrows next to the shells depict the orientation convention. The large black arrow in the upper right corner indicates the flow direction.

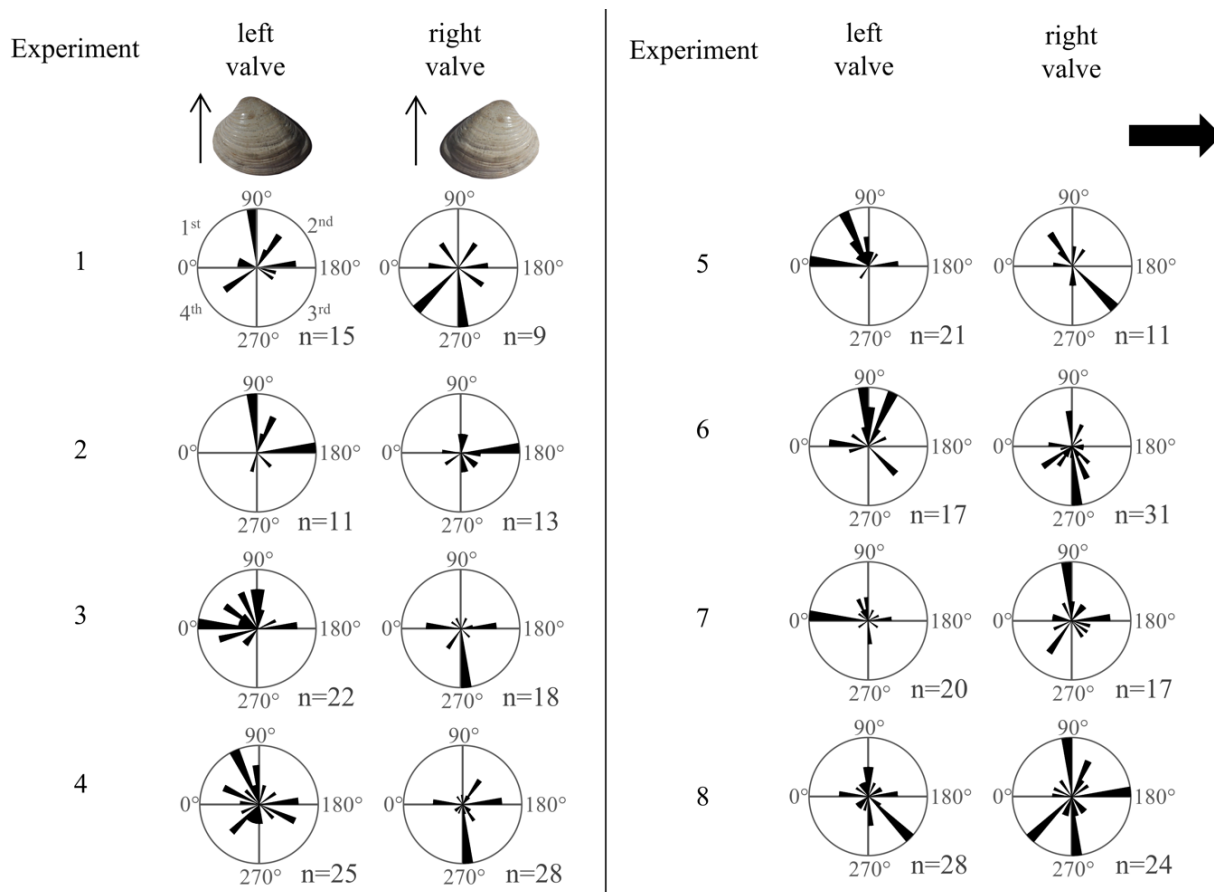


Figure 10. Umbo orientation of the shells in a compound bed of *Anomalocardia brasiliiana* right and left valves for the eight experiments. n: number of measurements; 0°: upstream flume side. The thin black arrows next to the shells depict the orientation convention. The large black arrow in the upper right corner indicates the flow direction.

Table 4. Umbo orientation results for the *Anomalocardia brasiliiana*: left and right valves.

Shell-bed experiment	Flow velocity (ms ⁻¹)	Left valves		Right valves	
		n	Quadrants first and second (%)	n	Quadrants third and fourth (%)
1	0.57	15	73.33	09	66.67
2		11	81.82	13	76.92
3		22	81.82	18	61.11
4		25	56.00	28	64.29
5	0.54	21	95.24	11	45.45
6		17	82.35	31	74.19
7		20	80.00	17	47.06
8		28	60.71	24	58.33
Average			76.41		61.75
Standard deviation			12.73		11.40

DISCUSSION

Threshold of motion

As reported by Futterer (1982) for some bivalve shells (*Glycymeris glycymeris* and *Mytilus edulis*), the results of this laboratory investigation demonstrated that shells in a convex-up position were hydrodynamically less stable when the umbo was pointing upstream. In this scenario, the shells began to move downstream while, at same time, rotating around their

vertical axes to adopt the more stable umbo-downstream position. Dey (2003) linked this rotational movement to the fact that an inertial movement is induced by an imbalance due to the protruding umbo.

Concerning the differences in the thresholds of motion between species, *Divaricella quadrisulcata* had smaller values of $\tau_{b,cr}$ and θ_{cr} in comparison to the other shells. One of the causes that can explain this behavior is the relationship between the shell mass (m) and its projected area facing the flow direction (S_{ac}).

Because the drag forces are a function of this area (Eq. 1), heavier grain particles with the same projected area will be more stable. This relationship (Fig. 11) showed upward curving trends, with that of *Divaricella quadrisulcata* having the least steepness ($R^2 = 0.97$; $m = 0.0013 S_{ac}^{1.42}$). *Anomalocardia brasiliiana* ($R^2 = 0.99$; $m = 0.0007 S_{ac}^{1.62}$) and *Codakia orbicularis* ($R^2 = 0.97$; $m = 0.0008 S_{ac}^{1.60}$) showed similar trends but with greater steepness than *Divaricella quadrisulcata*.

These thresholds of motion differences between species may be related to the results of Fornari (2010), who investigated a concentration of disarticulated, convex-up shells in a lagoonal facies of a Holocene back-barrier system located in the southern Brazilian coastal plain. In this case, the highest shell concentration was composed of *Anomalocardia brasiliiana* valves, which is an autochthonous species in that habitat.

The species *Divaricella quadrisulcata* and *Codakia orbicularis* (both native in shallow marine environments) occurred in overall smaller number wherein the former occurred more frequently than the latter. The fact that *Divaricella quadrisulcata* has lower values of critical shear stress may be one of the factors that explains its higher concentration among the allochthonous species, as the latter shallow marine species are considered to have been transported by the tidal flood currents.

Regarding the Shields parameter, all thresholds of motion data acquired in the present study were obtained from a transitional flow regime ($5 \leq Re^* \leq 70$) with θ_{cr} values far below those of the critical Shields (1936) curve. Incipient movement studies on beds composed of heterogeneous calcareous sand (Prager *et al.* 1996) and shell fragments (Paphitis *et al.* 2002, Weill *et al.* 2010, Rieux *et al.* 2019) have reported critical Shields parameter (θ_{cr}) between 8×10^{-3} and 4×10^{-2} for transitional flow regimes. These θ_{cr} values, which were also below the Shields curve, could be a consequence of the platy shape and density of some bioclastic particles (Prager *et al.* 1996). It should be noted that terrigenous materials composed of platy particles have lower thresholds of motion than the corresponding spherical ones, as observed by Mantz (1977) and Magalhães and Chau (1983) in cohesionless mica flakes and shale particles, respectively.

Fick *et al.* (2020) integrated some of these unidirectional flow data with their threshold of movement results for disarticulated bivalve and gastropod shells under oscillatory flow, generating an incipient shell bed motion envelope. The results from the present investigation, as well as those of Dey (2003) and Diedericks *et al.* (2018), showed that single shells in a bed composed of smaller particles (and roughness) had lower thresholds of motion under currents with θ_{cr} values (Fig. 8) lying below the Fick *et al.* (2020) envelope.

Theoretical models and experimental data (Egiazaroff 1965, Andrews 1983, Fisher *et al.* 1983, Wiberg and Smith 1987, Ramsdell and Miedema 2010) have indicated that for spherical grains, if the D/k_s ratios are lower than 1, an increase in the critical Shields parameter is obtained. When this ratio is greater than 1, the θ_{cr} values are displaced below the Shields (1936) curve. The present θ_{cr} values, which were below the Fick *et al.* (2020) envelope, can be explained by this relationship. In the case of Ramsdell and Miedema (2010), this is caused by the fact that the Shields parameter is inversely related to the particle diameter, while the boundary shear stress is only influenced by the change in velocity distribution. In addition, for natural sand, crushed quartzite, and glass spheres, Miller and Byrne (1966) experimentally verified that the repose angle (ψ_r) decreases with an increase in the D/k_s ratio. According to Eq. 4, this relationship suggests that the critical Shields parameter will be lower for larger D/k_s ratios.

The θ_{cr} scatter points for all three bivalve shells (Fig. 12) tested in this work, where the ratio (D/k_s) was between 15 and 25, show a good positive correlation ($R = 0.93$), with a coefficient of determination (R^2) of 0.86, and the thresholds of motion given by $\theta_{cr} = 9 \times 10^{-6} Re^{*1.83}$. The results are very similar to those reported by Dey (2003) ($R^2 = 0.80$; $\theta_{cr} = 9 \times 10^{-6} Re^{*1.88}$) under the same conditions. These trends are steeper than the curve ($D/k_s = 15$) by Ramsdell and Miedema (2010), crossing it at $Re^* \sim 25$.

The data points for the shells studied in this research, in which $6 < D/k_s < 15$ (Fig. 12), showed a larger scatter ($R^2 = 0.33$; $\theta_{cr} = 10^{-4} Re^{*1.15}$). Almost half of these data were between the regression curves ($D/k_s = 6$ and 15) of Ramsdell

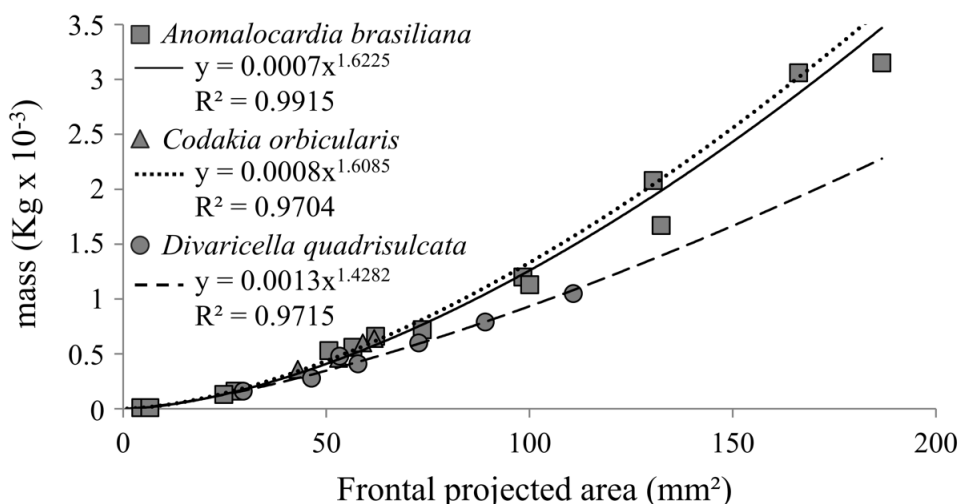


Figure 11. Shell mass as a function of projected shell areas in the direction of the flow (S_{ac}).

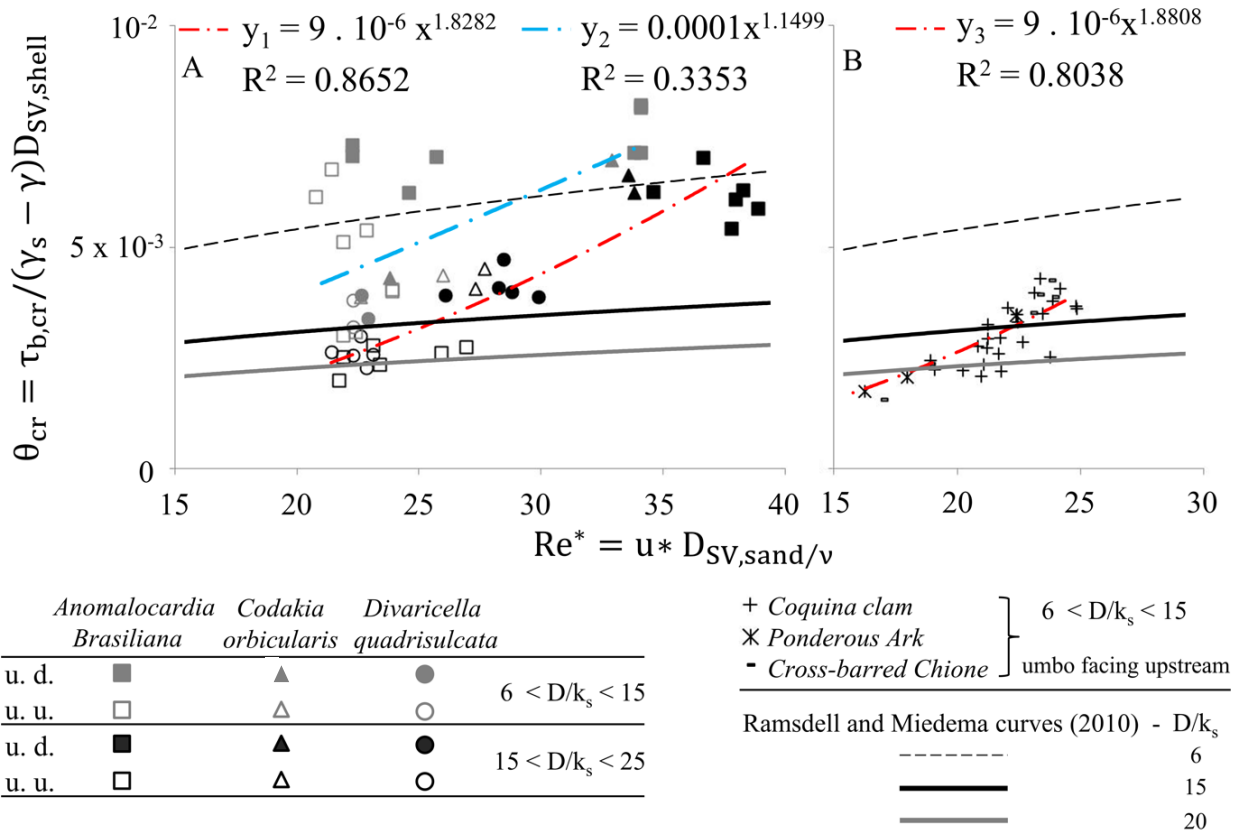


Figure 12. Critical Shields parameter (θ_{cr}) as a function of the grain Reynolds number (Re^*). (A) The results of this work discriminated between the shell species (*Anomalocardia brasiliiana*, *Codakia orbicularis*, and *Divaricella quadrisulcata*), initial umbo position (u.d.: umbo downstream; u.u.: umbo upstream) and D/k_s ranges (6–15, 15–25). Blue dashed line is the regression curve (y_2) for D/k_s between 6 and 15, red dashed line is the regression curve (y_1) for D/k_s between 15 and 25. (B) Results from Dey (2003) for the *Coquina clam* shells, *Ponderous Ark*, and transported in a convex-up/umbo upstream position with D/k_s ratio between *Cross-barred Chione* 6 and 15. Red dashed line is the regression curve (y_3). The Ramsdell and Miedema (2010) curves for D/k_s equal to 6, 15, and 20 are plotted on both graphs.

and Miedema (2010); however, there were also θ_{cr} values above the upper limit ($D/k_s = 6$).

Data from the literature show that beds made of carbonate particles have lower values of the critical Shields parameter than spherical siliciclastic grains when using the shell D_{sv} for the grain characteristic diameter. However, the results of this work, as well as the data from Dey (2003) and Diedericks *et al.* (2018), revealed that the same did not hold for nonuniform particles when comparing them with those of Ramsdell and Miedema (2010).

Shell orientation

The shell orientation results showed that elliptical and asymmetrical valves (*Anomalocardia brasiliiana*) that moved in a convex-up position tended to point the right valve umbo toward the right side of the flume and the left valve to the opposite side, thus producing a bimodal orientation pattern. This behavior, already described by Kidwell *et al.* (1986), did not occur in circular shells. From another point of view, *Anomalocardia brasiliiana* specimens have a longer axis parallel to the flow with the posterior end pointing downstream.

In addition, Newell *et al.* (2007) reported that the posterior sides of bivalve shells tend to face downstream (Fig. 13). The authors made more than 500 orientation measurements of the bivalve shell *Unio* sp. (elliptical asymmetric shape) in

convex-up positions in recent point-bar deposits. Although other data of elliptical bivalve shells in convex-up positions show that the long axis is parallel to the flow direction (Behrens and Watson 1969, Futterer 1982), the species *Donax variabilis* and *Petricola pholadiformis* have more stable positions with the posterior shell end pointing upstream. Elongated triangular shells (*Mytilus edulis*) also produce a long-axis orientation pattern parallel to the flow (convex-up transported), as seen by Kelling and Williams (1967) and Nagle (1967). These data demonstrate that the major axis is the main controller in the orientation of elongated shells: however, the bimodal pattern of umbo orientations in elliptical shell species reveals that the umbo produces a secondary effect in shell orientation.

The majority of shell orientation data comes from experiments conducted with the shell in a convex-up position because it is a hydrodynamically more stable position, as well as being the regular position of shells on rock surfaces or sediments in response to wave and current action (Bailey and Erickson 1973, Kreisa and Bambach 1982, Posenato *et al.* 2013). However, it is known that shells can be transported over short distances in concave-up positions until they flip over to adopt a more stable position (Brenchley and Newall 1970). Under such conditions, the transport orientation of the elongated shells differs distinctly from that of the convex-up shells, where the longer axis tends to stay perpendicular to the flow direction.

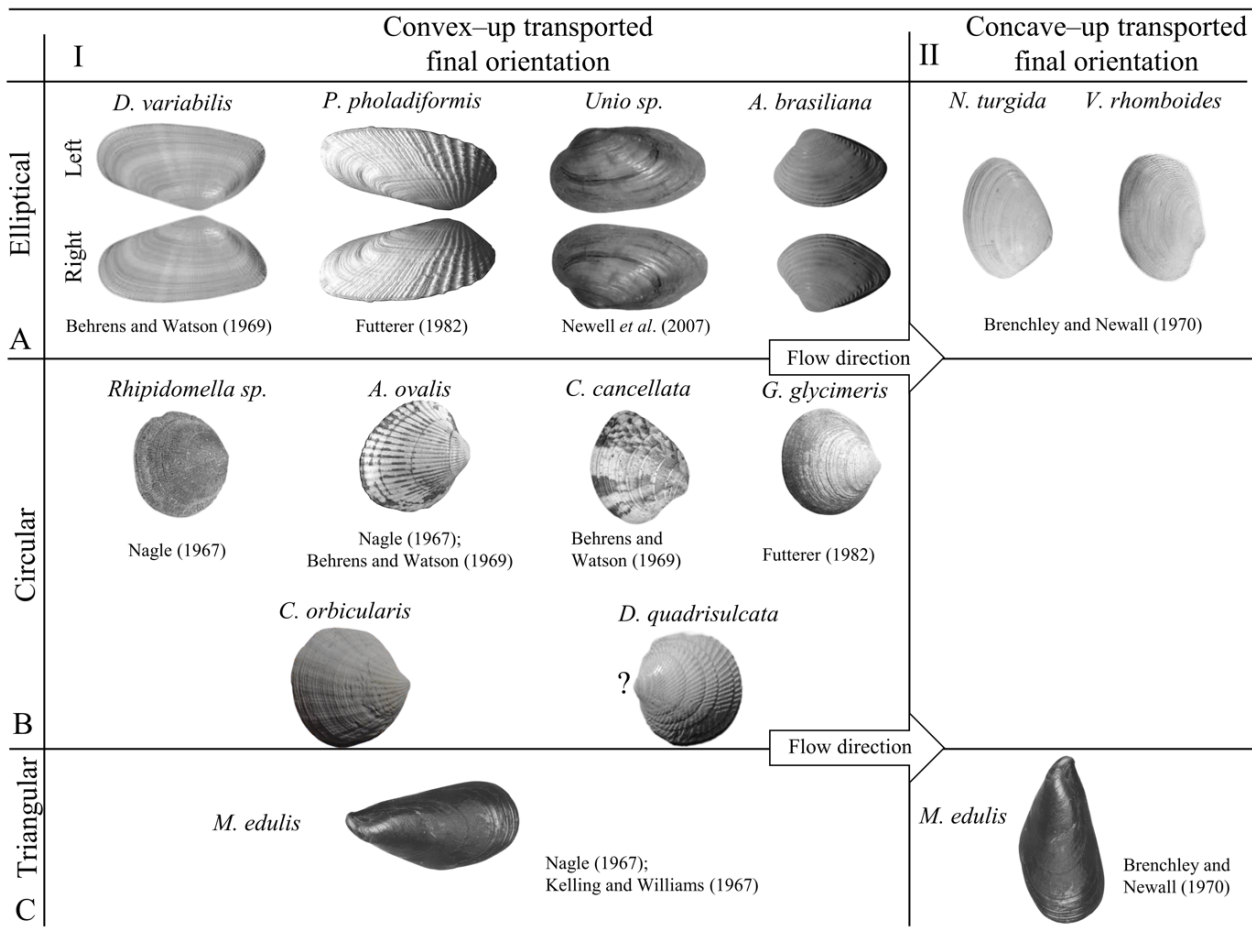


Figure 13. Shell orientation under unidirectional flow. (I) Final orientation of the shells transported in a convex-up initial position. (II) Final orientation of the shells transported in a concave-up initial position. (A) Elliptical shell shapes. (B) Circular shell shapes. (C) Triangular shell shapes. Question mark next to *D. quadrisulcata* refers to this species umbo orientation results pointing upstream which is in contrast with his more hydrodynamic position (umbo to downstream). The shell photographs are modified from Zenetos *et al.* (2009), Fassatoui *et al.* (2019) and World Register of Marine Species (2022).

The literature on the orientation of circular shells (*Rhipidomella sp.*, *Andara ovalis*, *Chione cancellata*, and *Glycymeris glycymeris*) moving in a convex-up position reveals that the umbo tends to point downstream (Nagle 1967, Behrens and Watson 1969, Futterer 1982). The *Codakia orbicularis* species' results agree with these data, as its threshold of motion data showed larger critical shear stress values for downstream facing umbos, and their umbo final orientation measurements also pointed in the flow direction. Although *Divaricella quadrisulcata* is more hydrodynamic when its umbo faces downstream, the final orientation measurements showed that when this species started to move with the umbo pointing upstream, it could maintain this orientation until its movement stopped. Due to these distinct observations, it is difficult to infer how *Divaricella quadrisulcata* valves would be oriented in the paleocurrent analysis.

CONCLUDING REMARKS

Using laboratory flumes, this research investigated the threshold of motion and final orientation of the bivalve shells *Anomalocardia brasiliiana*, *Codakia orbicularis*, and *Divaricella quadrisulcata* when transported by currents.

The thresholds of motion results achieved led to the following conclusions:

- Valves in a convex-up position are entrained at a higher flow energy when the umbo is initially pointing downstream rather than upstream;
- The threshold of motion differences between species can be related to the shell shape with regard to the relationship between the shell mass and frontal shell area facing the current;
- Shells transported over a bed of low roughness have critical transport thresholds well below the Shields curve;
- Elliptical shells transported in a convex-up position tend to be oriented with the long axis parallel to the flow, with the umbos of opposite valves pointing toward opposite flow margins (bimodal pattern). This pattern was observed in both scenarios tested in this research: single-shell and shell-bed experiments;
- Circular shells transported in a convex-up position tend to be oriented with the umbo pointing downstream;
- Valves transported in a convex-up position with their umbo initially pointing downstream will continue to move. However, when the umbo faces upstream, the shells rotate on a horizontal plane until a hydrodynamically more stable position is attained and then stop moving.

ACKNOWLEDGMENTS

We thank the Instituto de Pesquisas Hidráulicas (IPH), the Núcleo de Estudos de Correntes de Densidade (NECOD), and the Programa de Pós-Graduação em Geociências from the Universidade Federal do Rio Grande do Sul. We are thankful to Pré-Sal Petróleo S.A. (PPSA) and the Libra Group, a consortium comprising Petrobras, Shell Brazil, TotalEnergies, CNODC and CNOOC Limited, in partnership with UFRGS (Project 826-IPH/PETROBRAS 5850.0105486.17.9 COQUINAS) for their financial support to the first author with special thanks to Maria José Resende Oliveira (PETROBRAS/LIBRA/AT) and Jian Zhao (CNODC BRASIL PETRÓLEO E GÁS LTDA/LIBRA/AT). We also appreciate the valuable comments of the reviewer Marcello G. Simões.

NOMENCLATURE

A = wet area (m²)
 a = shell's longest axis (m)
 b = shell's intermediated axis (m)
 c = shell's inferior axis
 D_n = nominal diameter (m)

D_{sv} = sieve diameter (m)
 D/k_s = ratio between shell D_{sv} and mean bed D_{sv}
 F_D = drag force (N)
 F_L = lift force (N)
 h = flow depth (m)
 P = wet perimeter (m)
 Q = discharge (m³ s⁻¹)
 R = Pearson correlation coefficient
 R² = coefficient of determination
 Re* = grain's Reynolds number
 S = flume slope
 Sac = projected area on plan formed by axes a and c (m²).
 u_{*} = shear velocity (m s⁻¹)
 V = shell volume (m³)
 W = submerged weight (N)
 γ_s = specific weight of shell (N m⁻³)
 γ = specific weight of water (N m⁻³)
 θ_{cr} = critical Shields parameter
 ρ = specific mass of water (Kg m⁻³)
 ρ_s = specific mass of shell (kg m⁻³)
 τ_{b,cr} = critical shear stress (Pa)
 Ψ = bed slope angle
 Ψ_r = repose angle

ARTICLE INFORMATION

Manuscript ID: 20220080. Received on: 16 MAY 2022. Approved on: 15 FEB 2023.

How to cite this article: Silva F.R.S., Borges A.L.O., Toldo Jr. E.E., Fick C., Puhl E., Oliveira V.C.B., Cruz F.E.G. 2023. Threshold of motion and orientation of bivalve shells under current flow. *Brazilian Journal of Geology*, 53(1):e20220080. <https://doi.org/10.1590/2317-4889202320220080>

F.S.S.: Conceptualization, Data curation, Formal Analysis, Investigation, Methodology, Writing — original draft, Writing — review & editing. A.O.B.: Conceptualization, Data curation, Formal Analysis, Investigation, Methodology, Supervision, Validation, Visualization, Writing — review & editing. E.E.T.: Conceptualization, Supervision, Validation, Visualization, Writing — review & editing. C.F.: Validation, Visualization, Writing — review & editing. E.P.: Project administration, Supervision, Validation, Visualization, Writing — review & editing. V.O.: Funding acquisition, Validation, Project administration. F.C.: Funding acquisition, Validation, Project administration.

REFERENCES

- Allen J.R.L. 1984. Experiments on the terminal fall of the valves of bivalve molluscs loaded with sand trapped from a dispersion. *Sedimentary Geology*, 39(3-4):197-209. [https://doi.org/10.1016/0037-0738\(84\)90050-2](https://doi.org/10.1016/0037-0738(84)90050-2)
- Andrews E.D. 1983. Entrainment of gravel from naturally sorted riverbed material. *Geological Society of America Bulletin*, 94(10):1225-1231. [https://doi.org/10.1130/0016-7606\(1983\)94%3C1225:E0GFNS%3E2.0.CO;2](https://doi.org/10.1130/0016-7606(1983)94%3C1225:E0GFNS%3E2.0.CO;2)
- Bailey L.T., Erickson M.J. 1973. Preferred orientation of bivalve shells in the Upper Timber Lake Member, Fox Hills Formation in North Dakota - Preliminary interpretations. *The Compass of Sigma Gamma Epsilon*, 50(2):23-37.
- Behrens E.W., Watson R.L. 1969. Differential sorting of pelecypod valves in the swash zone. *Journal of sedimentary Petrology*, 39(1):159-165.
- Brenchley P.J., Newall G. 1970. Flume experiments on the orientation and transport of models and shells valves. *Palaeogeography, Palaeoclimatology, Palaeoecology*, 7(3):185-220. [https://doi.org/10.1016/0031-0182\(70\)90093-3](https://doi.org/10.1016/0031-0182(70)90093-3)
- Buffington J.M., Montgomery D.R. 1997. A systematic analysis of eight decades of incipient motion studies, with special reference to gravel-bedded rivers. *Water Resources Research*, 33(8):1993-2029. <https://doi.org/10.1029/96WR03190>
- Calliari L.J., Klein A.H.F. 1993. Características morfodinâmicas e sedimentológicas das praias oceânicas entre Rio Grande e Chuí. *RS. Pesquisas*, 20(1):48-56. <https://doi.org/10.22456/1807-9806.21281>
- Carvalho M.D., Praça U.M., Silva-Telles A.C., Jahnert R.J., Dias J.L. 2000. Bioclastic carbonate lacustrine facies models in the Campos Basin (Lower Cretaceous), Brazil. *American Association of Petroleum Geologists, Studies in Geology*, 46:245-256. <https://doi.org/10.1306/St46706C19>
- Charó M.P., Gordillo S., Fucks E.E., Giaconi L.M. 2014. Late Quaternary molluscs from the northern San Matias Gulf (Northern Patagonia, Argentina), southwestern Atlantic: faunistic changes and paleoenvironmental interpretation. *Quaternary International*, 352:26-47. <https://doi.org/10.1016/j.quaint.2013.12.044>
- Chattopadhyay D., Rathie A., Das A. 2013. The effect of morphology on postmortem transportation of bivalves and its taphonomic implications. *Palaios*, 28(3-4):203-209.
- Church M.A., McLean D.G., Wolcott J.F. 1987. River bed gravels: Sampling and analysis. In: Thorne C.R., Bathurst J.C., Hey R.D. (eds.). *Sediment Transport in Gravel-bed Rivers*. Chichester: Wiley, p. 43-88.
- Dey S. 2003. Incipient motion of bivalve shells on sand beds under flowing water. *Journal of Engineering Mechanics*, 129(2):232-240. [https://doi.org/10.1061/\(ASCE\)0733-9399\(2003\)129:2\(232\)](https://doi.org/10.1061/(ASCE)0733-9399(2003)129:2(232))
- Diedericks G.P.J., Troch C.C.A., Smit G.J.F. 2018. Incipient motion of shells and shell Gravel. *Journal of Hydraulic Engineering*, 144(3):1-9. [https://doi.org/10.1061/\(ASCE\)HY.1943-7900.0001421](https://doi.org/10.1061/(ASCE)HY.1943-7900.0001421)

- Egiazaroff I. 1965. Calculation of non-uniform sediment concentrations. *Journal of the Hydraulic Division*, **91**(4):225-247. <https://doi.org/10.1061/JYCEAJ.0001277>
- Fassatoui C., Jenhani A.B.R., Romdhane M.S. 2019. Relative growth, shell morphology and genetic relationships between freshwater mussels of the genus *Unio* (Mollusca: Bivalvia: Unionidae) from rivers of the Ichkeul watershed (Tunisia). *Molluscan Research*, **39**(4):313-324. <https://doi.org/10.1080/13235818.2019.1631958>
- Fick C., Puhl E., Toldo E.E. 2020. Threshold of motion of bivalve and gastropod shells under oscillatory flow in flume experiments. *Sedimentology*, **67**(1):627-648. <https://doi.org/10.1111/sed.12657>
- Fisher J., Sill B., Clark D. 1983. Organic detritus particles: initiation of motion criteria on sand and gravel beds. *Water Resources Research*, **19**(6):1627-1631. <https://doi.org/10.1029/WR019i006p01627>
- Fornari M. 2010. *Evolução sedimentar holocênica da retrobarreira na região de Jaguaruna-Laguna, Santa Catarina, Brasil*. PhD Thesis, Universidade de São Paulo, São Paulo, 262 p.
- Futterer E. 1982. Experiments on the distinction of wave and current influenced shell accumulations. In: Einsele G., Seilacher A. (Eds.). *Cyclic and Event Stratification*. Berlin-Heidelberg: Springer, p. 175-179.
- Jahnert R., Paula O., Collins L., Strobach E., Pevzner R. 2012. Evolution of a coquina barrier in Shark Bay, Australia by GPR imaging: architecture of a Holocene reservoir analog. *Sedimentary Geology*, **281**:59-74. <https://doi.org/10.1016/j.sedgeo.2012.08.009>
- Kelling G., Williams P.F. 1967. Flume studies of the reorientation of pebbles and shells. *The Journal of Geology*, **75**(3):243-267.
- Kidwell S.M., Fürsich F.T., Aigner T. 1986. Conceptual framework for the analysis and classification of fossil concentrations. *Palaios*, **1**(3):228-238. <https://doi.org/10.2307/3514687>
- Kreisa R.D., Bambach R.K. 1982. The role of storm processes in generating shell beds in Paleozoic shelf environments. In: Einsele, G., Seilacher, A. (Eds.), *Cyclic and Event Stratification*. Berlin-Heidelberg: Springer, p. 200-207.
- Li Y., Yu Q., Gao S., Flemming B.W. 2020. Settling velocity and drag coefficient of platy shell fragments. *Sedimentology*, **67**(4):2095-2110. <https://doi.org/10.1111/sed.12696>
- Magalhães L., Chau T.S. 1983. Initiation of motion conditions for shale sediments. *Canadian Journal of Civil Engineering*, **10**(3):549-554. <https://doi.org/10.1139/L83-081>
- Mantz P.A. 1977. Incipient transport of fine grains and flakes by fluids extended Shields diagram. *Journal of the Hydraulics Division*, **103**(6):601-615. <https://doi.org/10.1061/JYCEAJ.0004766>
- Middleton G.V. 1967. The orientation of concavo-convex particles deposited from experimental turbidity currents. *Journal of Sedimentary Petrology*, **37**:229-239.
- Miller M.C., McCave I.N., Komar P.D. 1977. Threshold of sediment motion under unidirectional currents. *Sedimentology*, **24**(4):507-527. <https://doi.org/10.1111/j.1365-3091.1977.tb00136.x>
- Miller R., Byrne R. 1966. The angle of repose for a single grain on a fixed rough bed. *Sedimentology*, **6**(4):303-314. <https://doi.org/10.1111/j.1365-3091.1966.tb01897.x>
- Muniz M.C., Bosence D.W.J. 2018. Lacustrine carbonate platforms: Facies, cycles, and tectonosedimentary models for the presalt Lagoa Feia Group (Lower Cretaceous), Campos Basin, Brazil. *AAPG Bulletin*, **102**(12):2569-2597. <https://doi.org/10.1306/0511181620617087>
- Nagle J.S. 1967. Wave and current orientation of shells. *Journal of Sedimentary Petrology*, **37**(4):1124-1138. <https://doi.org/10.1306/74D71848-2B21-11D7-8648000102C1865D>
- Newell A.J., Gower D.J., Benton M.J., Tverdokhlebov V.P. 2007. Bedload abrasion and the in situ fragmentation of bivalve shells. *Sedimentology*, **54**(4):835-845. <https://doi.org/10.1111/j.1365-3091.2007.00862.x>
- Oliveira V.C.B., Silva C.M.A., Borghi L.F., Carvalho I.S. 2019. Lacustrine coquinas and hybrid deposits from rift phase: Pre-Salt, lower Cretaceous, Campos Basin, Brazil. *Journal of South American Earth Sciences*, **95**:102254. <https://doi.org/10.1016/j.jsames.2019.102254>
- Olivera A.M., Wood W.L. 1997. Hydrodynamics of bivalve shell entrainment and transport. *Journal of Sedimentary Research*, **67**(3):514-526. <https://doi.org/10.1306/D42685B8-2B26-11D7-8648000102C1865D>
- Paphitis D., Collins M.B., Nash L.A., Wallbridge S. 2002. Settling velocities and entrainment thresholds of biogenic sands shell fragments under unidirectional flow. *Sedimentology*, **49**(1):211-225. <https://doi.org/10.1046/j.1365-3091.2002.00446.x>
- Posenato R., Bassi D., Avanzini M. 2013. Bivalve pavements from shallow-water blackshales in the Early Jurassic of northern Italy: a record of salinity and oxygen depleted environmental dynamics. *Palaeogeography, Palaeoclimatology, Palaeoecology*, **369**:262-271. <https://doi.org/10.1016/j.palaeo.2012.10.032>
- Prager E.J., Southard J.B., Vivoni-Gallart E.R. 1996. Experiments on the entrainment threshold of well-sorted and poorly sorted carbonate sands. *Sedimentology*, **43**(1):33-40. <https://doi.org/10.1111/j.1365-3091.1996.tb01457.x>
- Radley J.D. 2011. Biostratigraphic signature of Penarth Group (Upper Triassic) shell concentrations (Severn Estuary, South-West England): A preliminary account. *Geoscience in South-West England*, **12**(4):351-355.
- Ramsdell R.C., Miedema S.A. 2010. Hydraulic transport of sand/shell mixtures. In: World Dredging Congress, 19., 2010, Beijing. *Proceedings...* p. 1039-1059.
- Rieux A., Weill P., Mouaz D., Poirier P., Nechenache F., Perez L., Tessier B. 2019. Threshold of motion and settling velocities of mollusc shell debris: Influence of faunal composition. *Sedimentology*, **66**(3):895-916. <https://doi.org/10.1111/sed.12521>
- Rodrigues M.G., Varejão F.G., Matos S.A., Fürsich F.T., Warren L.V., Assine M.L., Simões M.G. 2022. High-resolution taphonomy and sequence stratigraphy of internally complex, bivalve-dominated coquinas from the Aptian Romualdo Formation, Araripe Basin, NE Brazil. *Marine and Petroleum Geology*, **143**:105814. <https://doi.org/10.1016/j.marpetgeo.2022.105814>
- Schwartz T.M., Graham S.A. 2015. Stratigraphic architecture of a tide-influenced shelf-edge delta, Upper Cretaceous Dorotea Formation, Magallanes-Austral Basin, Patagonia. *Sedimentology*, **62**(4):1039-1077. <https://doi.org/10.1111/sed.12176>
- Shields A. 1936. *Application of similarity principles and turbulence research to bedload movement*. Publication no. 167. Pasadena: Hydrodynamics Laboratory, California Institute of Technology, 36 p.
- Smith D.A., Cheung K.F. 2004. Initiation of Motion of Calcareous Sand. *Journal of Hydraulic Engineering*, **130**(5):467-472. [https://doi.org/10.1061/\(ASCE\)0733-9429\(2004\)130:5\(467\)](https://doi.org/10.1061/(ASCE)0733-9429(2004)130:5(467))
- Tavares A.C., Borghi L.F., Corbett P., Nobre-Lopes J., Câmara R. 2015. Facies and depositional environments for the coquinas of the Morro do Chaves Formation, Sergipe-Alagoas Basin, defined by taphonomic and compositional criteria. *Brazilian Journal of Geology*, **45**(3):415-429. <https://doi.org/10.1590/2317-488920150030211>
- Trewin N.H., Welsh W. 1972. Transport, breakage and sorting of the bivalve *Macra corallina* on Aberdeen beach, Scotland. *Palaeogeography, Palaeoclimatology, Palaeoecology*, **12**(3):193-204. [https://doi.org/10.1016/0031-0182\(72\)90059-4](https://doi.org/10.1016/0031-0182(72)90059-4)
- Vogel S. 1994. *Life in Moving Fluids*. New Jersey: Princeton University Press, 467 p.
- Weill P., Mouazé D., Tessier B. 2013. Internal architecture and evolution of bioclastic beach ridges in a megatidal chenier plain: Field data and wave flume experiment. *Sedimentology*, **60**(5):1213-1230. <https://doi.org/10.1111/sed.12027>
- Weill P., Mouazé D., Tessier B., Brun-Cottan J.C. 2010. Hydrodynamic behavior of coarse bioclastic sand from shelly cheniers. *Earth Surface Processes and Landforms*, **35**(14):1642-1654. <https://doi.org/10.1002/esp.2004>
- Wendt J. 1995. Shell directions as a tool in palaeocurrent analysis. *Sedimentary Geology*, **95**(3-4):161-186. [https://doi.org/10.1016/0037-0738\(94\)00104-3](https://doi.org/10.1016/0037-0738(94)00104-3)
- Wiberg P.L., Smith J.D. 1987. Calculations of the critical shear stress for motion of uniform and heterogeneous sediments. *Water Resources Research*, **23**:1471-1480. <https://doi.org/10.1029/WR023i008p01471>
- World Register of Marine Species. *An authoritative classification and catalogue of marine names*. World Register of Marine Species. Available at: <https://www.marinespecies.org/>. Accessed on: May 6, 2022.
- Zenetos A., Ovalis P., Vardala-Theodorou E. 2009. The American piddock *Petricola pholidiformis* Lamarck, 1818 spreading in the Mediterranean Sea. *Aquatic Invasions*, **4**(2):385-387. <https://doi.org/10.3391/ai.2009.4.2.15>